engineering proceedings

MDPI

Proceedings

Influence of Frequency-Sweeping on Discrete and Continuous Phase Distributions Generated in Alkali-Metal Vapours

Abu Mohamed Alhasan [1,2,*,‡] and Salah Abdulrhmann[3,*]

[1] Physics Department, Faculty of Science, Assiut University, Assiut 71516, Egypt.
[2] Bağlar Mahallesi, 31500 Ryhanlı, Hatay, Turkey.
[3] Department of Physics, Faculty of Science, Jazan University, P.O. Box 114, 45142 Jazan, Saudi Arabia.
* Correspondence: am.alhasan.sq@gmail.com and sabdulrhmann@jazanu.edu.sa
† Presented at the 4th International Electronic Conference on Applied Sciences, 27 October–10 November 2023; Available online: https://asec2023.sciforum.net/.
‡ Retired.

Abstract: This paper establishes a comparable study on the influence of frequency-sweeping on discrete and continuous phase distributions associated with pulse excitations for a double-lambda atomic system in alkali metal vapours with a hyperfine structure. The excitation dynamics provided a different scheme of sigmoidal types and the optical pulses are assumed to be Gaussians. We shall focus on the set-up of electromagnetically induced transparency (EIT). The phases of optical fields give similarities to discrete square wave distributions influenced by ramping. The results showed significant control of discrete phase distributions and temporal ramping by sigmoidal membership functions implementation. The relevant equations are the reduced Maxwell equations for the radiation fields, and the density matrix equation in the Liouville space governs the time evolution.

Keywords: electromagnetically-induced transparency; continuous frequency-sweeping; stepped frequency-sweeping; sigmoidal membership functions implementation; alkali-metal vapours; D_1 line; hyperfine structure

1. Introduction

In recent papers, we have studied the temporal profile associated with the phases of dual-color pulses, such as the drive and the probe train in a double-lambda system composed of the hyperfine states of alkali atoms with a nuclear spin I = 3/2 [1,2]. The field's phases were shown to form temporal discrete distributions such as square waves. The significant parameters were the detuning of the upper hyperfine levels and the atomic radiative relaxations. Here, we are interested in temporal discrete and continuous phase distributions, which characterize the interaction with time-dependent frequency sweeping for both drive and probe fields. The frequency scanned across the splitting of the upper hyperfine levels. The shape of frequency-sweeping is given in terms of sigmoidal-type membership functions (SMF) [3]. The benefits of using SMF rely on the fact that it contains two member functions to control the shape of the sigmoid function. We aim in such a way to manipulate the temporal profile of the field's phases. Allen and Eberly obtained an analytical solution for two-level Bloch equations and deduced the sech pulse for the field envelope where they used tanh frequency-sweeping [4]. Recently, Kaviani et al. analyzed sweeping the resonance frequency of two-level atoms in an adiabatic regime [5]. They showed that the atomic frequency-sweeping (AFS) memory has similarities to EIT-based memories in quantum storage and retrieval of light experiments.

The proposed approach in this paper attempts to generalize the foundations of Al-

Citation: To be added by editorial staff during production.

Academic Editor: Firstname Lastname

Published: date

len and Eberly [4] to the case of multilevel atoms interacting with polychromatic electromagnetic fields. We further implement a dual-frequency frequency-sweeping on the optical transitions of the lower-lambda system. That is to study their impact on the phases without appealing to the polaritons concept introduced by Fleischhauer and Lukin [6] and applied by Kaviani et al to the case of sweeping the atomic frequency in quantum storage and retrieval of light [5].

2. The Atomic System and its Optical Excitation Scheme

In this section, we analyze a double-lambda configuration with a two-color excitation of ^{87}Rb atom within the D_1 line, i.e. 5s $^2S_{1/2}$ − 5p $^2P_{1/2}$ [2]. The bar states are described in terms of the generic four states: $|1\rangle = |5\ ^2S_{1/2}(F_g = 1)\rangle$; $|2\rangle = |5\ ^2S_{1/2}(F_g = 2)\rangle$; $|3\rangle = |5\ ^2P_{1/2}(F_e = 1)\rangle$; $|4\rangle = |5\ ^2P_{1/2}(F_e = 1)\rangle$, where F_g (F_e) stands for the total angular momentum associated with ground and excited hyperfine states. The probe filed is tuned to the transition $1 \leftrightarrow 3$, and the drive filed is tuned to the transition $2 \leftrightarrow 3$. The $1 \leftrightarrow 2$ is a dipole forbidden-transition.

The hyperfine-splitting of the ground and excited states is denoted by $\Delta\omega_g$ and $\Delta\omega_e$, respectively. The Rabi frequency for the probe and drive transition is described by Ω_p and Ω_r, respectively. In the following, we consider working in relative units. $\Omega(\Delta\omega)$ is the Rabi frequency (detuning) in units of γ, the spontaneous decay rate of the excited atomic state, $^2P_{1/2}$. Whereas the normalized distance ζ and the normalized retarded-time τ are measured in units of the Beers length of one of the pulses and the excited atomic-state lifetime, respectively. We take the spectroscopic data of ^{87}Rb from [7]. In the present work, the configuration of the probe-drive is different from the case of chirped stimulated rapid adiabatic passage considered by Chathanathi et al. [8]. We have kept only the one-photon detuning as a function of time, while the two-photon detuning is compensated by the instantaneous chirping of the probe and drive. The probe and drive one-photon time-dependent detuning are defined as

$$\delta_p(t) = \omega_p(t) - \omega_{31},$$
$$\delta_r(t) = \omega_r(t) - \omega_{32}, \quad (1)$$

where ω_p and ω_r stand for the instantaneous angular frequency of the probe and drive, with the atomic transition angular frequency ω_{31} and ω_{32}. We aim to scan the frequency across the upper hyperfine splitting $\Delta\omega_e$. We set $\omega_p(0) = \omega_{31}$ and $\omega_r(0) = \omega_{32}$. The frequency sweeping will not undershoot or overshoot the upper hyperfine splitting. Therefore, the endpoints of the sweep are well-defined as pointed out by Sawyer et al [9].

We choose the function *S(T, a, b)* as in the Matlab sigmoidal membership function [3]. Its first argument T represents the interaction time domain $T = [\tau_0, \tau_f]$, where τ_0 and τ_f denote the initial and final time considered. The function *S(T, a, b)* contains two membership functions that control the time profile and the approach to unity for final times. Therefore the frequency-sweeping can be rewritten as

$$\delta_p(T, a, b) = \Delta\omega_e * S_p(T, a, b),$$
$$\delta_r(T, a, b) = \Delta\omega_e * S_r(T, a, b). \quad (2)$$

Finally, the instantaneous sweeping $\Delta_{a,b}(\tau)$ can be written as the interpolation of $\delta(T, a, b)$ at the moment τ

$$\Delta_{a,b}(\tau) = \text{spline}(T, \delta(T, a, b), \tau). \quad (3)$$

Figure 1 presents the frequency-sweeping $\Delta_{a,b}(\tau)$ as a function of time for different membership functions of the sigmoidal-type excitation.

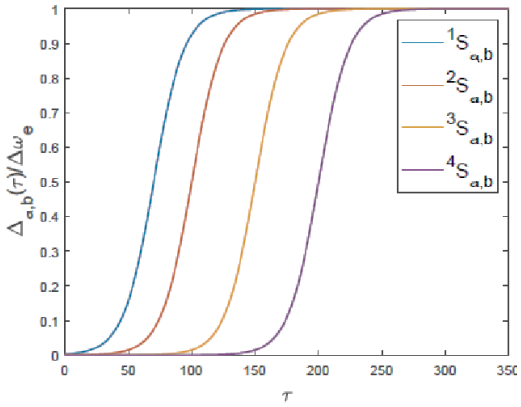

Figure 1. The frequency-sweeping function $\Delta_{a,b}(\tau)$ in the course of time for different membership functions a and b with the assessments:1, a = 0.0841, b = 70; 2, a = 0.0841, b = 100; 3, a = 0.0841, b = 150; 4, a = 0.0841, b = 200

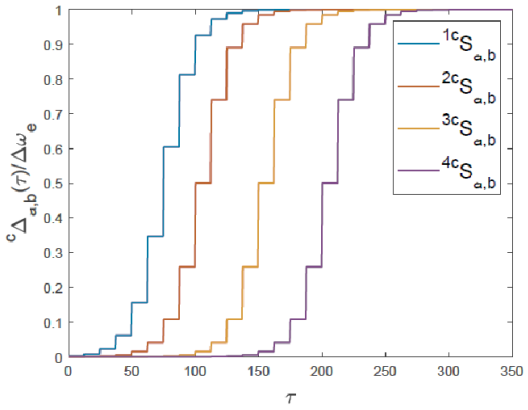

Figure 2. The chopped frequency-sweeping function $^c\Delta_{a,b}(\tau)$ in the course of time for different membership functions a and b with the assessments:1, a = 0.0841, b = 70; 2, a = 0.0841, b = 100; 3, a = 0.0841, b = 150; 4, a = 0.0841, b = 200. The chopping time interval $\Delta\tau$ = 12.5.

Figure 2 depicts the chopping of the frequency-sweeping function at a constant time step $\Delta\tau$ = 12.5. 76

The time evolution of the reduced density matrix ρ_s(t) is given by the first-order Liouville-von Neumann differential equation

$$-i\,\frac{\partial\rho_s(\tau)}{\partial t} = \hat{\mathcal{L}}_t\rho_s(\tau),\quad \hbar = 1, \tag{4}$$

where $\hat{\mathcal{L}}_t$ stands for the Liouvillian super-operator in the Liouville space [10,11].

The reduced-Maxwell equations are related to the two-component polarizations of rank one: $\rho_{3,1}^{(10)}, \rho_{4,1}^{(10)}$ and $\rho_{3,2}^{(10)}, \rho_{4,2}^{(10)}$ associated with probe and drive transitions as

$$\begin{aligned}\frac{\partial}{\partial\zeta}\Omega_p(\zeta,\tau) &= \sqrt{8/6}\,[\rho_{3,1}^{(10)}(\zeta,\tau) - \sqrt{5}\rho_{4,1}^{(10)}(\zeta,\tau)],\\ \frac{\partial}{\partial\zeta}\Omega_r(\zeta,\tau) &= \sqrt{8/2}\,[\rho_{3,2}^{(10)}(\zeta,\tau) - \rho_{4,2}^{(10)}(\zeta,\tau)],\end{aligned} \tag{5}$$

where m = 0 for the magnetic quantum number. The probe and drive are linearly polarized and propagate co-linearly.

The time evolution of the density matrix can be described as

$$\frac{\partial}{\partial\tau}\rho(\tau) = L(\Gamma^k, \Delta\omega_e, \Delta\omega_g, {}^p\Delta_{a,b}(\tau), {}^r\Delta_{a,b}, \tfrac{\Omega_p}{\sqrt{8}}, \tfrac{\Omega_r}{\sqrt{8}})\,\rho(\tau), \tag{6}$$

where Γ^k is the relative relaxation rate components of rank k, and L is the Liouvillian matrix [11]. Let $^r\Delta_{a,b}(\tau)$ and $^p\Delta_{a,b}(\tau)$ refer to the time-dependent detuning for the drive and probe, respectively.

3. Numerical Results

Throughout this study, we shall restrict ourselves to the response of rubidium atoms. Other alkalines like sodium and potassium give quite different time-dependent phase distributions indicating strong dependence on the upper hyperfine splitting and the atomic relaxations. Figure 3 depicts the temporal behavior of the inject pulses at ζ = 0 in black curves for the probe and drive. The initial temporal pulse profiles for the probe and drive are assumed to be Gaussian. In this paper, we have truncated the initial interaction time to contain two probe fields only instead of three, as done in [1,2]. Furthermore, we have kept the domain of the time-axis to be the same. Long-time behavior manifests the ring field response, yielding significant ramping in the phase distributions. Alhasan et al. discussed the influence of the ring field on the propagation stability of ultra-short pulses in duplicated two-level atoms media [12].

3.1. Pulse Profiles, Energy, Phase, and Propagation

Figure 4 shows the drive and probe temporal pulse profiles at the final distance considered, $\zeta = 21$. Black curves present the reference pulses without chirping at $\zeta = 0$.

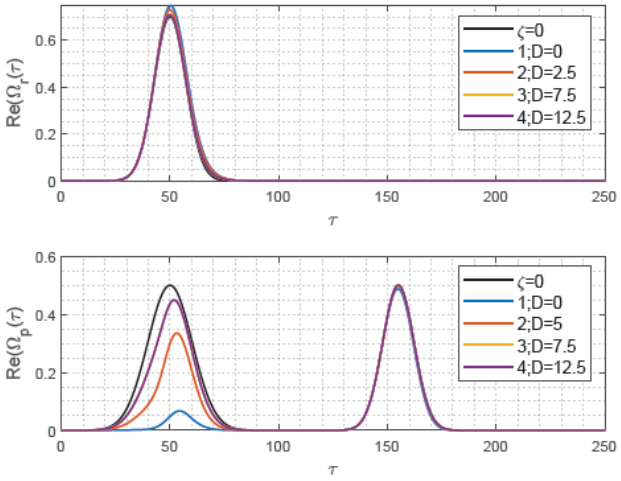

Figure 3. Drive and probe temporal pulse profiles. Black curves correspond to the reference pulses without chirping at $\zeta = 0$, and various colors correspond to the final distance at $\zeta = 21$. The effect of sweeping is considered for the third case with ${}^{3}S_{a,b}$ and ${}^{3}\Delta_{a,b}$ at different time-chopping steps $D = \Delta\tau = 0$, 5 , 7.5, and 12.5.

The effect of sweeping is considered for the third case with ${}^{3}S_{a,b}$ and ${}^{3}\Delta_{a,b}$ at different chirping, as presented in Figure 3. Drive field maxima at $\zeta = 21$ are close to the injected pulse at $\zeta = 0$. Let us compare the relative energies at $\zeta = 21$ for different chirping as

$$[{}^{a_1,b_1}E_r\ {}^{a_2,b_2}E_r\ {}^{a_3,b_3}E_r\ {}^{a_4,b_4}E_r\ ] = [1.0000\ 1.1031\ 1.0334\ 1.0333] \quad (7)$$

There is a tendency to increase the energy of the drive pulse as it is frequency-swept off the resonance frequency. There is strong absorption in the first probe pulse without chirping. The transparency increased as the probe pulses off-resonant through chirping. The transparency for the second probe in the train for large swept off-resonances is remarkable. Figure 4 shows the enhancements of the imaginary part of the probe pulses. Such an effect is responsible for the phase production. Let us define the time section $T_1(\tau) = [0, 180]$ as the effective duration-time of the pulses with the atomic medium without its tail. The initial interval, $T_0(\tau) = [0, 70]$, is omitted since the field response is so small, and the phase takes the initial constant value of 0π. In Figure 5, we have considered presenting the phases' temporal shape of the probe train for different locations inside the medium and for chopping time intervals: $\Delta\tau = 0$, 5, 7.5, and 12.5. The discrete phase distributions are evident for small distances like $\zeta = 2$. The phase jumps to build up at $\tau_1 = 100$ as the final time required to finish the interaction with the first probe pulses. The second phase discontinuity starts at time $\tau_2 = 120$, and it defines the time as the interaction with the second probe pulse in the train starts up. Beyond the second interaction time, the phases remain at constant values, i.e. for $\tau \in [120, 180]$. In Figure 5(a), we have distinguished discrete distributions associated with various colors as

1. black : $\{0\pi, -1\pi, 0\pi\}$; with chopping time interval $\Delta\tau = 0$,
2. blue : $\{0\pi, 1\pi, 2\pi\}$; with chopping time interval $\Delta\tau = 5$,
3. red : $\{0\pi, 1\pi, 0\pi\}$; with chopping time interval $\Delta\tau = 7.5$,
4. green : $\{0\pi, 1\pi, 2\pi\}$; with chopping time interval $\Delta\tau = 12.5$.

For moderate distances as in Figure 5(b), we have distinguished the continuous and discrete combinations as

1. black : $\{\epsilon_1(\tau), 0\pi, -1\pi, 0\pi\}$,
2. red : $\{0\pi, -1\pi, 0\pi\}$,
3. green : $\{\epsilon_2(\tau), 1\pi, 2\pi\}$.

The function $\epsilon_1(\tau)$ grows in a small interval but eventually collapses to 0π phases. While the function $\epsilon_2(\tau)$ grows up and ends with π values.

In Figure 5(d), the blue curve overrides the black curve, leaving distinct limiting cases such as $\{-2\pi, 0\pi, 2\pi\}$.

Figure 6 depicts the long-time behavior of temporal phases as the extended-time response for the ring field after the dominant existence of the pulses. Ring fields expose phase-ramping through short stepping and yielding phase mutations. Finally, limiting phases are stabilized. Intermediate chopping time intervals $\Delta\tau$ = 5, and 7.5 (blue and red curves) give substantial phases as -7π, and -10π, respectively.

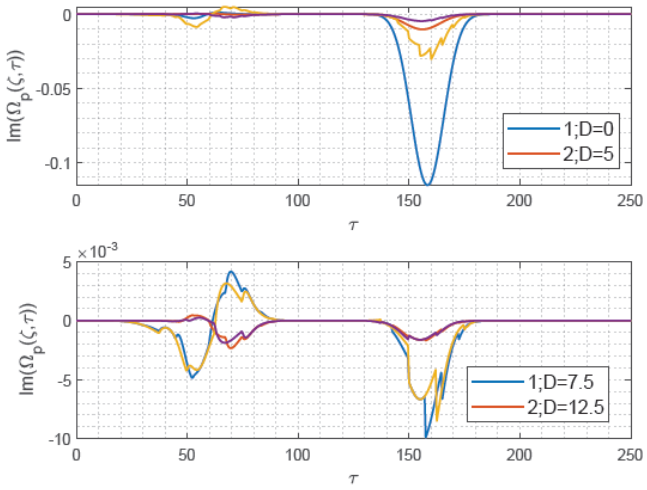

Figure 4. Temporal profile for drive and probe pulses where the effect of sweeping has been considered for the third case, ${}^3S_{a,b}$ and ${}^3\Delta_{a,b}$. Together with different chopping times at the finial distance ζ = 21.

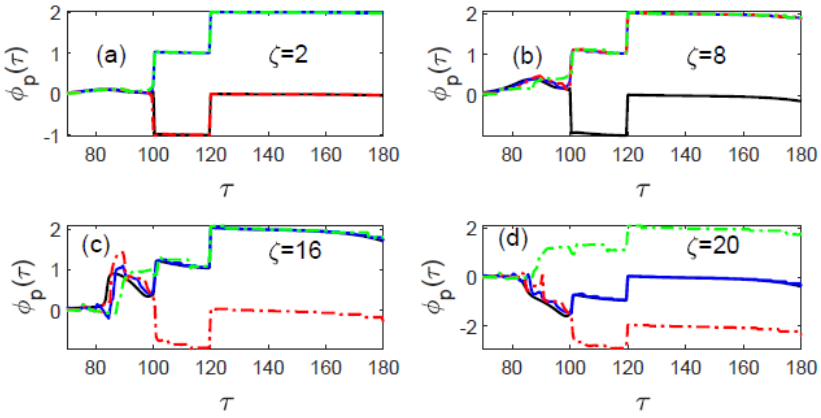

Figure 5. Phase profile corresponding to interaction-time for the probe pulse at different distances, where the effect of sweeping is considered for the third case, ${}^3S_{a,b}$ and ${}^3\Delta_{a,b}$, at various chopping times. The chopping time interval $\Delta\tau$ = 0, 5, 7.5, and 12.5 for black, blue, red and green curves, respectively.

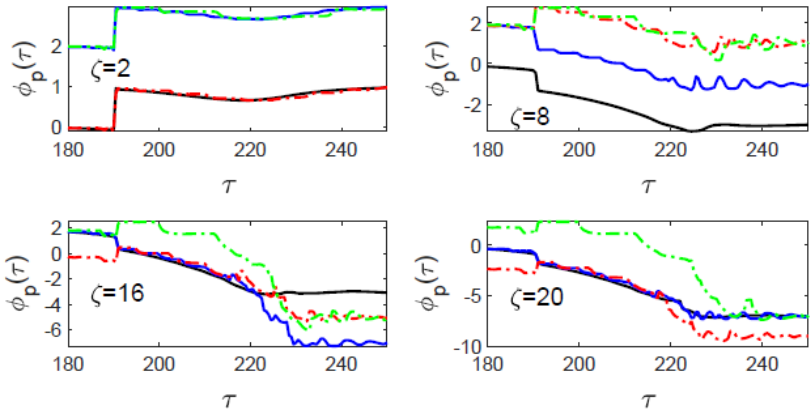

Figure 6. Extended-time phase profile for the probe pulse at different distances, where the effect of sweeping is considered for the third case, ${}^3S_{a,b}$ and ${}^3\Delta_{a,b}$, at various chopping times. The chopping time interval $\Delta\tau$ = 0, 5, 7.5, and 12.5 for black, blue, red and green curves, respectively.

4. Conclusions

We have discussed the phase response of a dual-color pulse excitation in alkaline vapours with a hyperfine structure. The pulses are frequency-swept within the upper hyperfine splitting, similarly. The sweeping excitation is a sigmoidal-type function with two membership functions to control the final time achievement and adjust the sweeping rate. We have also analyzed the influence of increasing chopping time intervals on phase generation and stabilization within propagation inside the medium. We calculated the phases for one of the alkaline vapors, mainly rubidium. The distribution of phases is different for different alkaline due to the strong dependence on the upper hyperfine splitting and the atomic relaxation. The numerical results showed that the phases were categorized into two distinctive distributions: discrete and continuous, with a superposition of discrete or continuous ramping mutations. For a small distance, we obtained two-phase discontinuities. Beyond discontinuities, the phases maintained a constant value. We identified eight phase distributions for different chopping intervals. These distributions are produced during the pulse's mean length. We have notified another type of phase generated due to the ring field for long-time response and asymptotic behavior for far distances. Ring fields expose phase-ramping through short stepping and producing phase mutations with substantial phases as -7π, and -10π.

Author Contributions: Conceptualization, A.M.A.; methodology, A.M.A. and S.A.; software, A.M.A. and S.A.; validation, A.M.A. and S.A.; formal analysis, A.M.A. and S.A.; investigation, A.M.A. and S.A.; resources, A.M.A. and S.A.; data curation, A.M.A. and S.A.; writing—original draft preparation, A.M.A.; writing—review and editing, A.M.A. and S.A.; visualization, A.M.A. and S.A.; supervision, A.M.A.; project administration, A.M.A. All authors have read and agreed to the published version of the manuscript.

Funding: "This research received no external funding"

Conflicts of Interest: "The authors declare no conflict of interest."

References

1. Alhasan, A.M.; Abdulrhmann, S. Multilevel Phase Switch Generation in Alkali Vapors. Eng. Proc. **2023**, 31(1):69.
2. Alhasan, A.M.; Altowyan, A.S.; Madkhli, A.Y.; Abdulrhmann, S. Multiple Phase Stepping Generation in Alkali Metal Atoms: A Comparative Theoretical Study. Applied Sciences **2023**, 13(6):3670.
3. Sigmoidal membership function. Available online: https://www.mathworks.com/help/fuzzy/sigmf.html (accessed on 2023)
4. Allen, L; Eberly, J. Optical Resonance and Two-Level Atoms, New York, 1975; pp. 101–104.
5. Kaviani, H; Khazali, M; Ghobadi, R; Zahedinejad, E; Heshami, K; Simon, K. Quantum storage and retrieval of light by sweeping the atomic frequency. New J. Phys. **2013**, 15, 085029.
6. Fleischhauer, M.; Lukin, M. D. Quantum memory for photons: Dark-state polaritons. Phys. Rev. A **2002**, 65, 022314.
7. Steck, D. A. Rubidium 87 D Line Data. Available on-line at http://steck.us/alkalidata (Version 2.2.2, last revised 9 July 2021).

8. Chathanathil, J., Ramaswamy, A., Malinovsky, V. S., Budker, D., Malinovskaya, S. A. (2023). Chirped Fractional Stimulated Raman Adiabatic Passage. arXiv preprint arXiv:2305.18652.
9. Sawyer, B.J., Chilcott, M., Thomas, R. et al. Deterministic quantum state transfer of atoms in a random magnetic field. Eur. Phys. J. D **2019** 73, 160.
10. Fiutak, J.; van Kranendonk, J. The effect of collisions on resonance fluorescence and Rayleigh scattering at high intensities. J. Phys. B At. Mol. Phys. **1980**, 13, 2869–2884.
11. Alhasan, A. M. Entropy Associated with Information Storage and Its Retrieval. Entropy **2015**, 17, 5920–5937.
12. Alhasan, A.M.; Czub, J.; Miklaszewski,W. Propagation of light pulses in a (j1 = 1/2) ↔ (j2 = 1/2) medium in the sharp-line limit. Phys. Rev. A **2009**, 80, 033809.